Application of Atomic Layer Deposition of Platinum to Solid Oxide Fuel Cells

Xirong Jiang,[†] Hong Huang,[‡,§] Friedrich B. Prinz,[‡,∥] and Stacey F. Bent*,[⊥]

Departments of Physics, Mechanical Engineering, Material Science and Engineering, and Chemical Engineering, Stanford University, Stanford, California 94305

Received November 21, 2007. Revised Manuscript Received February 29, 2008

In this study, atomic layer deposition (ALD) was used to deposit Pt thin films as an electrode/catalyst layer for solid oxide fuel cells. $I-V$ measurements were performed to determine the dependence of the fuel cell performance on the Pt film thickness at different operating temperatures. The measured fuel cell performance revealed that comparable peak power densities were achieved for ALD-deposited Pt anodes with only one-fifth of the platinum loading relative to dc-sputtered Pt anodes. The Pt films fabricated by dc sputtering and ALD had different microstructure, which accounted for the difference in their performance as a fuel cell anode. In addition to the continuous electrocatalyst layer, a micropatterned Pt structure was fabricated via area-selective ALD and used as a current collector grid/patterned catalyst for the fuel cells. An improvement of the fuel cell performance by a factor of 10 was observed using the Pt current collector grid/patterned catalyst integrated onto cathodic $La_{0.6}Sr_{0.4}Co_{0.2}Fe_{0.8}O_{3-\delta}$. The study suggests the potential to achieve improved performance and/or lower loadings using ALD for catalysts in fuel cells.

Introduction

A solid oxide fuel cell (SOFC) is an all-solid device that converts the chemical energy of fuels such as hydrogen or simple hydrocarbons into electricity through electrochemical processes. With the ever increasing concern over the future availability of alternative energy sources, there is significant interest in the research and development of SOFCs because of their unique advantages over traditional power generation technologies. First, the efficiency of SOFCs is inherently high because it is not limited by the Carnot efficiency of a heat engine. Second, in SOFCs, the choice of fuels is versatile, including hydrogen and simple hydrocarbons. Third, the greenhouse gas emissions from SOFCs are much lower than those emitted from conventional power plants. In addition, due to the operating temperature range of SOFCs, the fuel processor can be incorporated into the fuel cell stack, which enables innovative thermal integration/management design features to provide excellent system efficiencies. Also, SOFCs can be used for cogeneration of steam or hot water, which if coupled with gas turbines to produce electrical power can enhance the overall system efficiency and range of applications.[1–6]

Current research activities in the development of SOFCs are increasingly focused on reducing their operating temperatures from traditional values near 1000 °C to lower temperatures of 500−800 °C. Such a reduction in operating temperature would lessen sealing problems, reduce performance degradation, and enable replacement of ceramic interconnects by cheaper metallic materials. However, a reduction of the operating temperature is detrimental from an electrochemical point of view. In general, fuel cells suffer from three major losses, including (a) activation loss arising from sluggish kinetics of the electrochemical charge-transfer reactions at the electrodes, (b) ohmic loss mainly stemming from slow ionic conduction in the electrolyte, and (c) concentration loss originating from the limited mass transport at high current densities.[2,7] At reduced operating temperature, the thermally activated electrode reactions and ion transport in the electrolyte become slower, resulting in lowered fuel cell performance. To reduce ohmic losses at reduced temperatures, an electrolyte with higher ionic conductivity or a thinner electrolyte structure is required. As the electrolyte resistance decreases, the overall cell losses then become dominated by the kinetics of electrochemical reactions at the anode and cathode.[4,5,8–10] Therefore, the electrode material requires particular attention in the development and optimization of low-temperature SOFCs.

Pt is well known for its chemical stability and excellent electrical properties at high temperatures, leading to enor-

* To whom correspondence should be addressed. Phone: 001 650 723 0385. Fax: 001 650 723 9780. E-mail: sbent@stanford.edu.
[†] Department of Physics.
[‡] Department of Mechanical Engineering.
[§] Current address: Department of Mechanical and Materials Engineering, Wright State University, 3640 Colonel Glenn Hwy, Dayton, OH 45435.
[∥] Department of Material Science and Engineering.
[⊥] Department of Chemical Engineering.

(1) Ralph, J. M.; Rossignol, C.; Kumar, R. *J. Electrochem. Soc.* **2003**, *150*, A1518.
(2) O'Hayre, R.; Cha, S.; Colella, W.; Prinz, F. B. *Fuel Cell Fundamentals*; John Wiley and Sons: New York, 2006.
(3) Steele, B. C. H.; Heinzel, A. *Nature* **2001**, *414*, 345.
(4) Jiang, S. P.; Chan, S. H. *J. Mater. Sci.* **2004**, *39*, 4405.
(5) Fleig, J. *Annu. Rev. Mater. Res.* **2003**, *33*, 361.
(6) *Fuel Cell Handbook*; U. S. Department of Energy; EG&G Technical Services, Inc. : Morgantown, WV, 2004.
(7) Carrette, L.; Friedlich, K. A.; Stimming, U. *Fuel Cells* **2001**, *1*, 1.
(8) Lashtabeg, A.; Skinner, S. J. *J. Mater. Chem.* **2006**, *16*, 3161.
(9) Huang, H.; Nakamura, M.; Su, P.; Fasching, R.; Saito, Y.; Prinz, F. B. *J. Electrochem. Soc.* **2007**, *154*, B20.
(10) Mazumder, S. K.; Acharya, K.; Haynes, C. L.; Williams, R.; von Spakovsky, M. R.; Nelson, D. J.; Rancruel, D. F.; Hartvigsen, J.; Gemmen, R. S. *IEEE Trans. Power Electron.* **2004**, *19*, 1263.

10.1021/cm7033189 CCC: $40.75
Published on Web 05/23/2008

mous application prospects in catalysis and microelectronics.[11,12] Pt has been reported to have excellent catalytic activity for the O_2 reduction reaction and the H_2 oxidation reaction at the electrode/electrolyte interface of an SOFC even at low operating temperatures.[6] When Pt is used as the catalytic material/cathode, the oxygen reduction reaction is dominated by the electrode surface path and bulk diffusion of oxygen is negligible. Thus, maximizing the surface area (triple phase boundary) while minimizing the Pt bulk is beneficial. Meanwhile, sufficient electrical connectivity in the electrode is required, putting severe limitations on Pt film thickness by traditional deposition methods. Therefore, to maintain catalytic activity while minimizing the loading of the noble metal Pt, atomic layer deposition (ALD), a nanoscale thin film deposition method, may prove to be a promising technique. The self-limiting adsorption reactions of the ALD process ensure precise control of film thickness, conformality, and uniformity over a large area. In addition to the application of ALD to the electrode/catalyst layer, the SOFC current collector provides another attractive target for ALD as a means to improve the fuel cell power efficiency. Patterned current collectors and microelectrodes prepared by lithography and atomic etching have been reported by several groups for various applications.[13–15] Here we use the technique of area-selective ALD, a method for depositing materials in a well-controlled pattern at the surface,[16–18] to fabricate a current collector consisting of a Pt grid pattern.

In this paper, we report the deposition of Pt thin films by ALD to be used as an electrocatalyst layer. The ALD-deposited Pt films are compared to their dc-sputtered counterparts to better understand the origin of differences in the fuel cell performance between the two methods. We also detail the fabrication of a micropatterned Pt structure for the current collector grids of the fuel cells through the technique of area-selective ALD. In the area-selective ALD process used here, a self-assembled monolayer (SAM), in particular, octadecyltrichlorosilane (ODTS), is used as the ALD resist to modify the chemical properties of the substrate surface for patterning. Finally, we describe the positive impacts of these Pt electrode/catalyst and Pt current collector grids on the SOFC performance of yttria-stabilized zirconia (YSZ)-based SOFCs.

Experimental Section

Chemical Reagents and Preparation of Si and YSZ Substrates. All chemical reagents, including octadecyltrichlorosilane (ODTS) (97%), toluene (anhydrous, 99.8%), and chloroform (99%), used to form SAMs were purchased from Aldrich. Poly(dimethylsiloxane) (PDMS) (Sylgard 184) was purchased from Dow Corning. The (methylcyclopentadienyl)trimethylplatinum (MeCpPtMe_3) (99%) precursor for ALD was obtained from Strem. All reagents and gases were used directly without further treatment. Nitrogen gas (99.9995%) was obtained from Praxair and purified by a gas filter from Nanochem (model no. PF-25) before use.

Si substrates were cut from Si(100) wafers purchased from Si-Tech, Inc. (p-type with boron dopant; resistivity of 1.0−10.0 Ω·cm) and cleaned by a standard piranha process, resulting in a chemical oxide-coated silicon substrate. Two types of YSZ substrates were used in this study. One was rf (radio frequency)-sputtered YSZ substrates deposited at 200 °C[19] and another was commercially available YSZ plates (Ceraflex). To clean the YSZ substrates, two steps were used.[20] First, the substrates were rinsed ultrasonically twice for 5 min in ethyl alcohol in order to remove grease. After the first rinse, the ethyl alcohol was renewed. Following the ethyl alcohol rinses, the YSZ membrane was exposed to an rf oxygen plasma for 10 min to make the surface hydrophilic. The counterpart for the ALD-deposited Pt films is a porous Pt film fabricated through dc sputtering at 10 Pa Ar pressure, 100 W, and room temperature.[9]

ALD and Area-Selective ALD of Pt. Pt thin films were deposited onto Si and YSZ substrates in a custom-built ALD flow reactor using (methylcyclopentadienyl)trimethylplatinum (MeCpPtMe_3) and air, providing a source of oxygen, as ALD precursors. A regular ALD cycle consisted of a 2 s exposure to MeCpPtMe_3, a 12 s N_2 purge, a 2 s exposure to dry air, and a 12 s N_2 purge. For the area-selective ALD process, the N_2 purging time after each precursor dose was extended to 30 s to ensure removal of any unreacted precursor or physisorbed byproduct from the substrate. In all of the ALD Pt processes, the Pt precursor temperature and substrate temperature were kept at 50 and 285 °C, respectively. The optimization procedures for both ALD experiments have been reported previously.[16–18]

The area-selective ALD procedure using microcontact printing, which was carried out in a dry glovebox, consists of three key steps as shown in Figure 1. First, PDMS stamps are fabricated through standard lithographic methods.[21] The master used to cast the PDMS stamp has a mesh structure containing lines and spacings of 2 and 4 μm, respectively. On each 1 cm × 1 cm area there are 16 separated mesh structures to match the fuel cell architecture described in the following paragraph. Second, the pattern encoded in the PDMS stamp is transferred via application of the SAM, produced from 10 mM ODTS solution in anhydrous toluene, onto the substrate by microcontact printing. Third, Pt thin films are selectively deposited by ALD onto areas of the substrate that are not deactivated by ODTS. If desired, the ODTS resist can be removed by ozone.

Film Characterization. The thicknesses of Pt films less than 5 nm were measured by single-wavelength ellipsometry (Gaertner Scientific Corp. L116C He−Ne), while films greater than 5 nm were measured by X-ray reflectometry (XRR). The incident angle for the ellipsometer is 70°. For Pt film, we use a refractive index of $n = 2.33$.[22]At larger thickness (>5 nm), absorption becomes significant, which may lead to inaccurate measurements with the ellipsometer. For the X-ray reflection measurements we used a PANalytical X'pert PRO X-ray diffraction system to do reflectometry analysis and obtain both the thickness and density of the ALD-deposited Pt thin films. Scanning electron micros-

(11) Sinfelt, J. *Catalysts Discoveries, Concepts, and Applications*; Wiley: New York, 1983.
(12) Sze, S. M., Ed. *VLSI Technology*; Mc Graw-Hill: New York, 1988.
(13) Fleig, J. *Solid State Ionics* **2003**, *161*, 279.
(14) Horita, T.; Yamaji, K.; Ishikawa, M.; Sakai, N.; Yokokawa, H.; Kawada, T.; Kato, T. *J. Electrochem. Soc.* **1998**, *145*, 3196.
(15) Horita, T.; Yamaji, K.; Sakai, N.; Yokokawa, H.; Kawada, T.; Kato, T. *Solid State Ionics* **2000**, *127*, 55.
(16) Jiang, X.; Bent, S. F. *J. Electrochem. Soc.* **2007**, *154*, D648.
(17) Jiang, X.; Bent, S. F. *ECS Trans.* **2007**, *3*, 249.
(18) Jiang, X.; Chen, R.; Bent, S. F. *Surf. Coat. Technol.* **2007**, *201*, 8799.
(19) Shim, J. H.; Chao, C.; Huang, H.; Prinz, F. B. *Chem. Mater.* **2007**, *19*, 3850.
(20) De Ridder, M.; Van Welzenis, R. G.; Brongersma, H. H. *Surf. Interface Anal.* **2002**, *33*, 309.
(21) Xia, Y.; Whitesides, G. M. *Angew. Chem., Int. Ed. Engl.* **1998**, *37*, 550.
(22) Lide, D. R. *CRC Handbook of Chemistry and Physics*; Taylor and Francis: Boca Raton, FL, 2007.

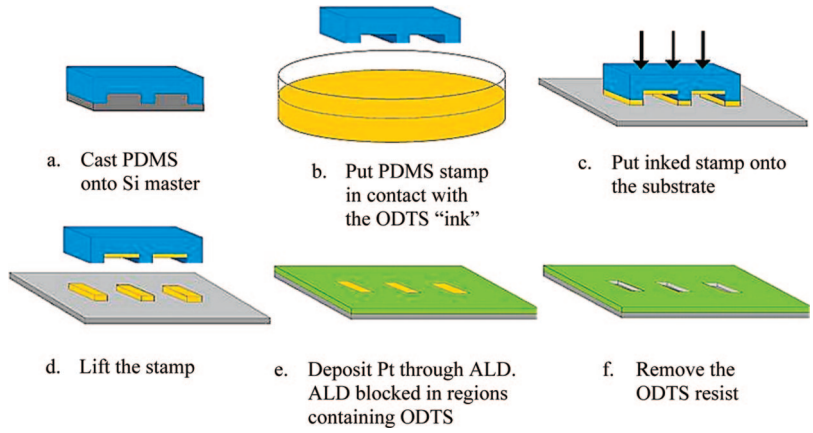

Figure 1. Schematic outline of the procedure to fabricate patterned Pt thin films using microcontact printing and selective atomic layer deposition.

copy (SEM) (FEI XL30 Sirion SEM with FEG source) and atomic force microscopy (AFM) (Digital Instruments Inc.) were used to determine the Pt film morphology. X-ray photoelectron spectroscopy (XPS) analysis was performed to investigate the film composition. The XPS system employed is an SSI S-Probe monochromatized spectrometer, which uses Al Kα radiation (1486 eV) as a probe. The instrument permits detection sensitivity of ~0.1 at. %. Auger electron spectroscopy (AES) (Evans Analytical Group) was used to look at the micropatterned Pt grid structures on YSZ. The AES instrument used in these studies has a spatial resolution of ~10 nm and a sensitivity of 0.1 at. % for Pt. Four-point probe measurement was used to determine the Pt film resistivity. Growth rate was determined by dividing the film thickness by the number of ALD cycles.

Thin SOFC Fabrication and Performance Characterization. To evaluate the properties of blanket-deposited ALD Pt in SOFC structures, the studies applied ALD platinum to the anode of a thin film SOFC test structure. The SOFC test structure was microfabricated on a silicon wafer, as described previously.[9] Briefly, the fabrication procedure started with coating both sides of a double-polished silicon wafer with a silicon nitride (Si_3N_4) layer to prevent electrical current leakage and avoid reaction between Si and YSZ. A YSZ film of 100 nm thick was then deposited by rf sputtering onto one side (top) of the wafer. On the other side (bottom), a partial area of the Si_3N_4 was removed using photolithography together with reactive ion etching (RIE). The opened Si windows were then etched with KOH, and the Si_3N_4 in the window structures was removed by RIE. The window size of the YSZ membrane was 100 μm × 100 μm. A porous platinum cathode of 80 nm thick was deposited on the top side of the YSZ membrane by dc sputtering with a shadow mask. Anodic platinum was then deposited on the bottom side, containing the window structure, by various methods depending on the desired experiment. For most experiments, a thin ALD Pt film was deposited to the desired thickness, ranging from 5 to 30 nm. During ALD of the anodic Pt, YSZ pieces were clamped to a piece of quartz in a special sample holder to prevent atomic layer deposition of Pt on the top side. Resistivity measurement confirmed that there was no significant deposition of Pt on the blocked side. Several fuel cells with dc-sputtered Pt anodes were prepared at the same time for comparison.

To evaluate the performance of the Pt grid feature as the current collector, we used SOFC test structures with thicker YSZ membranes, 50 μm, to provide sufficient mechanical strength for the microcontact printing process. Attempts to integrate the Pt grid onto thinner (50 and 100 nm thick) YSZ windows were unsuccessful because the YSZ membrane was broken during the stamping process. Thus, the thickness of the YSZ used for the stamping process was limited by the mechanical strength of the YSZ membrane, and 50 μm thick YSZ samples were chosen. Intermediate thicknesses between 100 nm and 50 μm were not investigated, so the minimum thickness limit for microcontact printing on these structures is not yet known.

The fabrication process for these Pt grid test structures differed from that described above. For these devices, dc-sputtered Pt of 80 nm thickness was used as the anode and 20 nm thick $La_{0.6}Sr_{0.4}Co_{0.2}Fe_{0.8}O_{3-\delta}$ (LSCF) was deposited by pulse laser deposition (PLD) with a shadow mask on the other side of a 50 μm thick YSZ plate (Ceraflex Co.) for the cathode. According to a separate SEM study, the PLD-deposited LSCF is fairly dense.[23] Subsequently, a 4.5 nm thick micropatterned Pt structure was fabricated through the area-selective ALD process onto the cathodic LSCF to examine the impact of the Pt grids on fuel cell performance. The increased YSZ membrane thickness of 50 μm will lead to very low fuel cell performance due to the large ohmic loss stemming from the thick electrolyte membrane. However, comparison between fuel cell performance with and without the Pt grids will still provide useful information on the impact of the Pt grids on the fuel cell.

After fabrication, the fuel cell structures were placed into a testing station. In this study, because we are exploring the suitability of ALD Pt as a catalyst/electrode layer for low-temperature SOFCs, we chose very low testing temperatures between 350 and 450 °C. In the testing station, the anode was linked to a gold gasket with an external electrical connection. The patterned cathode was connected via a microprobe manipulator capable of measuring individual fuel cells. Constant chamber temperature was maintained with the help of a temperature regulator. The temperature in the vicinity of the tested individual fuel cells was also monitored. $I-V$ data were collected with a Gamry instrument using the galvanodynamic (scanning current) mode.

Results and Discussion

ALD Pt Thin Films as the Anode in SOFCs. The ALD process for Pt has been previously described.[16,17] Here we review the key features. A linear dependence of film thickness on the number of ALD cycles was observed as shown in Figure 2a. The thickness of films greater than 5 nm was measured by X-ray reflectometry (XRR), while films thinner than 5 nm were measured by ellipsometry. This linear ALD growth supports the self-limiting growth mechanism of the ALD Pt process. The as-deposited Pt films were

(23) Crabb, K.; Prinz, F. B. Unpublished work.

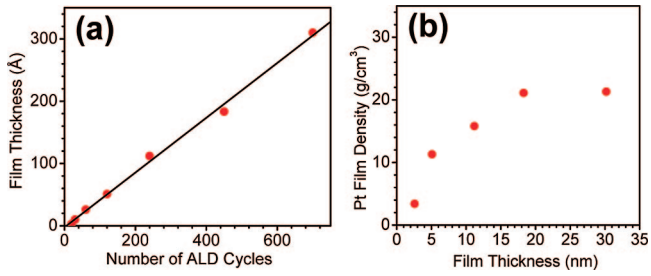

Figure 2. (a) Pt film thickness vs number of ALD cycles. (b) Film density of the as-deposited Pt film vs film thickness. ALD conditions: substrate temperature, 285 °C; precursor temperature, 50 °C; dosing time, 2 s; purge time, 12 s.

reported to be very pure based on X-ray photoelectron spectroscopy (XPS) studies. After removal of the topmost layers (~1 nm) by in situ argon ion sputtering, there were no observable impurities within the XPS sensitivity of 0.1%.[16,17] XRR was also employed to investigate the as-deposited Pt film density as a function of film thickness. Figure 2b shows that the film density increases with film thickness. For films thicker than 18.3 nm, the density reaches the bulk value, 21.4 g/cm^3, which indicates that Pt films thinner than 18.3 nm are discontinuous and/or porous, a morphology likely originating from the island growth mechanism.[24,25]

Given the large role of the film morphology on SOFC performance, studies of microstructure are important. It is also interesting to correlate microstructure and resistivity of as-deposited ALD Pt films upon annealing at elevated temperatures since the targeted operating temperatures of SOFCs are in the range of 300−550 °C. To reveal the dependence of the Pt microstructure on the film thickness, both high-resolution SEM and AFM techniques were employed. Figure 3a, 3b, and 3c show AFM images of 5, 10, and 30 nm thick as-deposited ALD Pt films. While the films were macroscopically uniform, the AFM images in Figure 3 show that the grain size increases with increasing film thickness. Figure 3d and 3f are the corresponding plan-view SEM images of the 10 and 30 nm thick as-deposited ALD Pt films, which verify the change of the surface morphology seen in the AFM images. Both the AFM and SEM images indicate that the roughness of the ALD-deposited Pt film increases with film thickness, which is due to the large grains that cover most of the surface. Substantially smaller grains cover the remainder of the surface.

The images also show a difference in film porosity as a function of film thickness. The SEM image of Figure 3e presents the 45° cross-sectional view of a 10 nm as-deposited ALD Pt film. The grain size of the 10 nm film is around 15 nm with a pore size of around 5 nm, and the porosity was estimated to be 10−20%. In contrast, Figure 3c and 3f shows that the 30 nm thick film is nearly continuous, and there are no obvious pores at this magnification of both SEM and AFM. There are, however, several pinholes in the 30 nm thick films, indicated by the dark spots in the images. For comparison, Figure 3g and 3h shows SEM images of the plan view and cross-sectional view of an 80 nm dc-sputtered

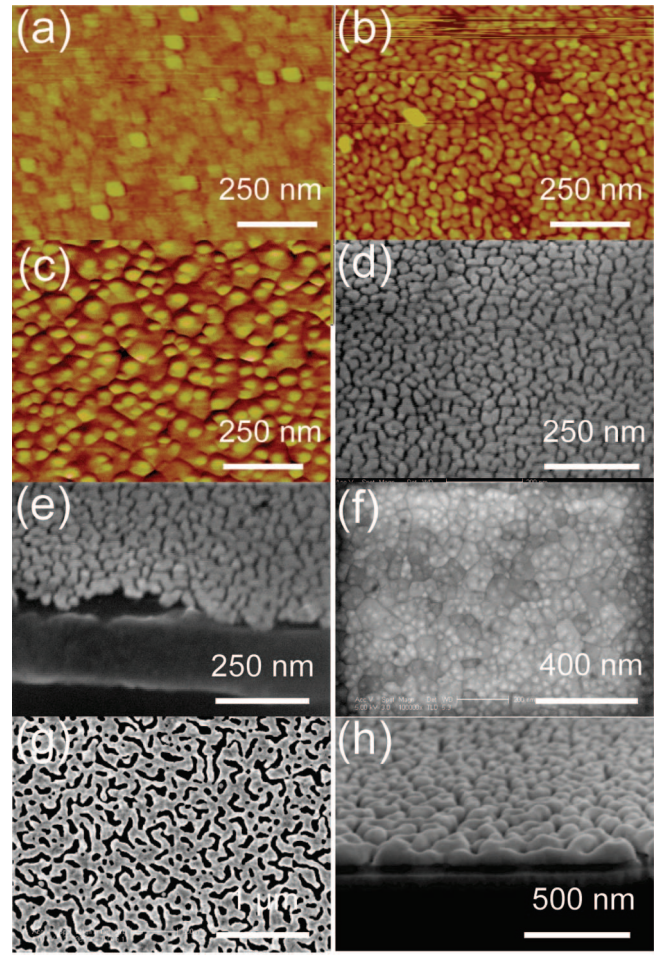

Figure 3. AFM images of (a) 5, (b) 10, and (c) 30 nm thick as-deposited ALD Pt films. SEM images of (d) plan view and (e) 45° cross-section view of a 10 nm as-deposited ALD Pt film. SEM image of (f) 30 nm thick as-deposited ALD film. SEM images of (g) plan view and (h) cross-section view of an 80 nm dc-sputtered Pt electrode. The vertical ranges of AFM images a, b, and c are 20, 8, and 18.7 nm, respectively.

Pt electrode. The microscopy shows that the Pt thin films deposited by dc sputtering are nanoporous. The pores in the Pt film are in the size range of 100 nm, and the porosity was estimated to be 30−40%, which is higher than that of the 10 nm ALD-deposited Pt film. The increased continuity of the ALD-deposited films over that of dc-sputtered films is expected due to the nature of the ALD process.[9,26–28]

To examine the temperature influences on the film morphology and resistivity, in this case simulating the cathode, a postannealing process was carried out in an O_2 environment for 30 min at each temperature. Table 1 lists the rms roughness and resistivity of both the as-deposited and the postannealed films at two different annealing temperatures (350 and 550 °C). The data show that the rms roughness of the postannealed films increases slightly compared to that of the as-deposited films. The resistivity of the ALD-deposited films is relatively low. For the as-deposited 30 nm thick Pt film, the resistivity is 18.3 $\mu\Omega\cdot$cm,

(24) Puurunen, R. L. *Chem. Vap. Depos.* **2003**, *9*, 327.
(25) Puurunen, R. L. *J. Appl. Phys.* **2005**, *97*, 121301.
(26) Suntola, T. *Handbook of Thin film Process Technology*; Institute of Physics: Bristol, U.K., 1995; Vol. 1.
(27) Leskela, M.; Ritala, M. *Angew. Chem., Int. Ed.* **2003**, *42*, 5548.
(28) Ritala, M.; Leskela, M.; Rauhala, E.; Haussalo, P. *J. Electrochem. Soc.* **1995**, *142*, 2731.

Table 1. RMS Roughness and Resistivity of As-Deposited and Postannealed Pt Films Measured by AFM and Four-Point Probe Method, Respectively[a]

	rms of Pt films on YSZ substrate (nm)			resistivity of Pt films on YSZ substrates ($\mu\Omega\cdot$cm)		
Pt film thickness (nm)	as deposited	350 °C	550 °C	as deposited	350 °C	550 °C
11.2	3.2	3.5	3.5	31.3	23.3	22.5
18.3	2.5	2.9	3.5	22.6	18.8	16.2
30	2.2	2.6	2.6	18.3	17.2	15.8

[a] Note: RMS roughness of YSZ substrate prior to deposition was 3.7 nm, and the resolution of the AFM is ~1 Å.

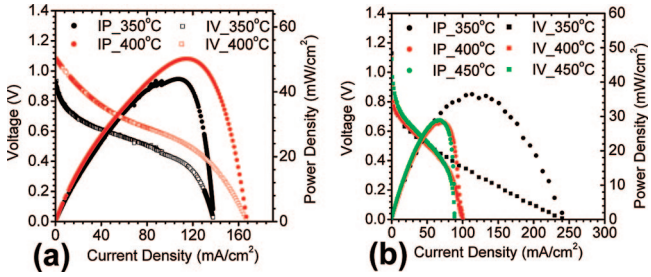

Figure 4. Characteristics of fuel cell performance. Fuel cells consisted of 100 nm thick RF-sputtered YSZ (electrolyte), 80 nm dc-sputtered Pt (cathode): (a) 10 nm ALD Pt anode and (b) 30 nm ALD Pt anode.

relatively higher than the bulk value (10.8 $\mu\Omega\cdot$cm). The observed high roughness and resultant high resistivity of the 11.2 nm ALD Pt films suggest a porous structure and hence high surface area, which may facilitate adsorption of O_2 and charge-transfer reactions as well as increase the triple phase boundaries. In the thicker film (30 nm), lower roughness and resistivity, especially after annealing at temperatures up to 550 °C, suggest more continuous microstructure, which is consistent with our AFM and SEM observation indicated in Figure 3c and 3f.

In the following, we will present the results of using ALD-deposited Pt thin films, with the properties described above, as the anode in ultrathin SOFCs at low operating temperatures. Figure 4a presents characteristic $I-V$ and $I-P$ curves of ultrathin SOFCs consisting of a 10 nm thick ALD Pt anode, 100 nm thick rf-sputtered YSZ electrolyte, and 80 nm thick dc-sputtered Pt cathode. At 350 °C, a peak power density as high as 45 ± 2 mW/cm^2 was obtained. When the operating temperature was increased to 400 °C, the peak power density increased to 50 ± 3 mW/cm^2. This enhanced performance at higher temperature arises because the thermally activated electrode reaction kinetics and ion transport in the electrolyte are improved at higher temperature. A secondary effect may be that the porosity of the Pt anode film increased during the fuel cell operation, as indicated by Figure 6b (see later discussion), potentially making it easier for the hydrogen fuel to reach the electrode/electrolyte interface.

Figure 4b shows the $I-V$ and $I-P$ curves of ultrathin SOFCs consisting of the same structure as in Figure 4a but with a 30 nm thick ALD Pt anode, measured at 350, 400, and 450 °C. Even though the thickness and microscopy measurements (see Figure 2b and Figure 3) indicate that 30 nm thick films are relatively dense, measurable fuel cell performance can still be detected. We postulate that performance persists for the 30 nm thick films because the hydrogen can penetrate through the pinholes observed in Figure 3c and 3f as well as along grain boundaries. At 350 °C, a peak power density of 38 ± 2 mW/cm^2 was achieved, which is lower than that of the 10 nm ALD Pt anode measured at the same temperature. The lower peak power density is expected since the porosity of the 30 nm film is lower compared to the 10 nm film, as determined in Figure 3. A denser anode catalyst layer makes diffusion of hydrogen more difficult and provides less triple phase boundary (TPB) for reaction, which leads to reduction of the performance.

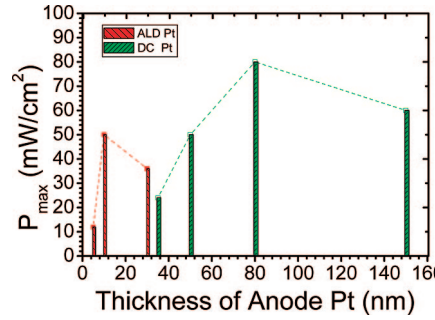

Figure 5. Dependence of fuel cell peak power densities on the thickness of anodic Pt deposited using ALD and dc-sputtering techniques. All data are from the initial measurement on SOFCs consisting of the same electrolyte and cathode structures (described in text) at 350 °C with a fuel flow rate of 10 sccm.

Interestingly, despite the increase in reaction and diffusion kinetics expected at higher temperatures, the peak power density for the 30 nm thick anode film was observed to decrease at operating temperatures of 400 and 450 °C. The decrease in peak power density can be traced to a rapid voltage drop at high current load, as seen in Figure 4b. In other words, for the higher temperature experiments, the characteristic concentration loss became dominant, leading to decreased power densities. The significant concentration loss observed here is most likely associated with starving of fuel at the interface of the electrode and YSZ electrolyte. As discussed earlier, at elevated temperature, the roughness and resistivity of ALD-deposited 30 nm Pt film is reduced due to formation of a more continuous microstructure, leading to less efficient diffusion of the reactant and product gases though an insufficiently porous film.

In addition to 10 and 30 nm ALD Pt films, SOFC performance with a 5 nm ALD Pt film was also investigated. The resistivity of the 5 nm as-deposited ALD Pt film is 51 $\mu\Omega\cdot$cm, which although higher than the resistivities shown in Table 1 is lower than that of the porous 80 nm dc-sputtered Pt film (134 $\mu\Omega\cdot$cm). Hence, the electrical connectivity suggests that the as-deposited 5 nm Pt film may form a good electrode for the SOFC. However, the lowest peak power density was obtained for the 5 nm thick ALD Pt anode film. We suspect that the poor fuel cell performance compared to thicker ALD Pt films is due in part to a rapid loss of electrical connectivity during fuel cell operation caused by degradation of the film. As discussed below, loss of connectivity is observed for 10 nm Pt anode films during operation; we speculate that the effect may be even worse for the thinner 5 nm Pt film. To utilize the catalytic activity of such a thin

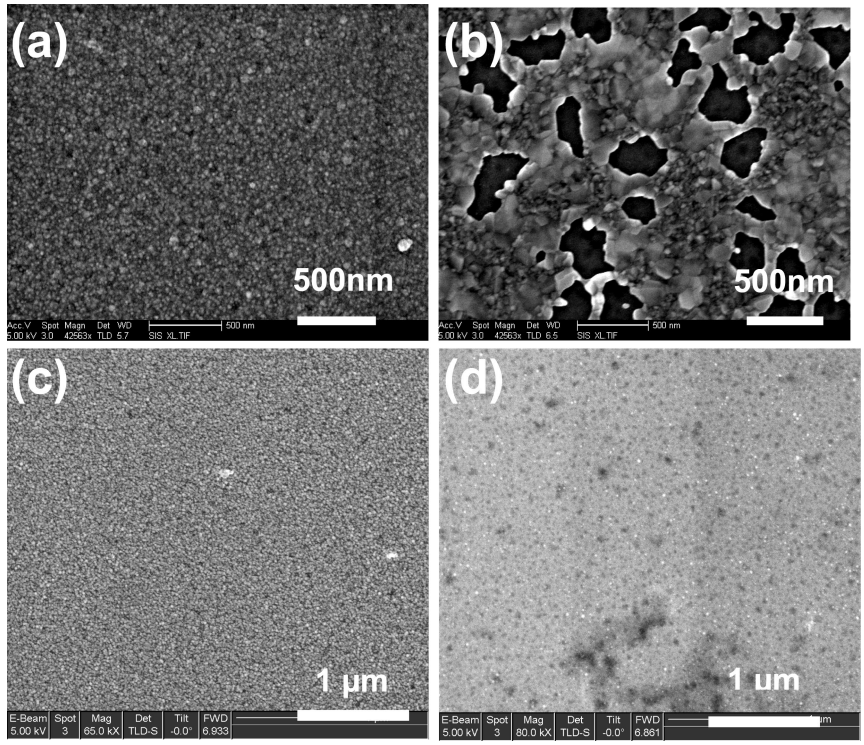

Figure 6. SEM images of 10 nm anode films (a) before and (b) after testing at 350 °C; SEM images of 30 nm Pt anode film (c) before and (d) after testing at 350 °C.

layer of Pt, another porous interconnected electronic conductor will likely be necessary to sustain electrical conduction.

It is interesting to compare the differences in fuel cell performance between the anodic Pt films fabricated through ALD and through dc sputtering. In Figure 5, the dependence of peak power density on the film thickness is summarized for both ALD Pt and dc-sputtered Pt anode. Figure 5 clearly shows that the fuel cell performance is very sensitive to the anode film thickness. Among the three different thicknesses studied in the current experiments, 10 nm is the preferred thickness for the ALD-deposited Pt films. The results suggest that the optimal thickness should be further explored around this value. In contrast, the optimal thickness using dc-sputtered Pt was found to be around 80 nm. Moreover, it takes 50 nm of sputter-deposited Pt to achieve similar power densities as achieved for 10 nm ALD Pt, indicating a 5 times reduction in loading necessary for ALD Pt. The smaller thickness needed for ALD films compared to sputtered films likely originates from the differences in their film microstructures. As discussed earlier, ALD-deposited Pt films are relatively dense by 30 nm, negatively impacting fuel diffusivity through the thin film. For the 10 nm ALD-deposited film, the pore size is around 5 nm and the porosity was estimated to be 15−20%, while the pores of the 80 nm dc-sputtered Pt film are around 100 nm and the porosity was estimated to be 30−40%. Only thinner ALD-deposited films can achieve comparable fuel diffusivity compared to its dc-sputtered counterpart. On the other hand, comparable fuel cell performance was achieved for ALD-deposited Pt anodes with only one-fifth of the platinum loading relative to dc-sputtered Pt anodes. From this point of view, the ALD technique can significantly reduce the Pt loading in SOFCs, which is a key criterion in reducing material cost.

Figure 6a−d exhibits SEM images of 10 and 30 nm thick ALD-deposited Pt anode films before and after fuel cell performance testing. As discussed above, the grain size of the 10 nm thick film is around 25 nm, on average, according to AFM and SEM analysis, and nanoscale pores exist. The microscopy results are consistent with the XRR analysis of Figure 2b, showing that a 10 nm thick Pt film has reduced density. These pores provide pathways through which H_2 gas can permeate, consistent with the $I-V$ results of Figure 4a taken at 350 °C for a fresh sample. However, after fuel cell testing for a prolonged time, the morphologies of the ALD Pt film changed significantly. In the 10 nm Pt film, the nanopores grew into larger pores with a diameter of 100−300 nm (Figure 6b). Formation of such large pores is associated with Pt coarsening under thermodynamic driving force. It might also be related to accumulation of the water reaction product at the interface of the anode and electrolyte during the fuel cell operation. In contrast, the 30 nm thick Pt anode became more dense and smooth with fewer pores after testing (see Figure 6d). Such an anode film morphology blocks H_2 diffusion in and water gas product diffusion out and will lead to concentration loss in the fuel cell. The change of the Pt microstructure occurring during operation hence affects the performance of the fuel cells in two ways: by changing the porosity and electrical connectivity. For the thinner anode film, the performance may increase with the increase of the porosity initially; however, as the pore size continued to increase, the loss of electrical connection may become a major factor which will damage fuel cell performance. This might offer an interpretation of the low performance observed using the 5 nm Pt electrodes.

Area-Selective ALD for Cathodic Electrical Grids in SOFCs. Another application of ALD in the SOFC device is to deposit Pt (or another metal) as a current collector. If Pt is used for this purpose, it can act both as the current collector and as the catalyst. The geometry that we explored in this application is the commonly used grid structure; this geometry will reduce the Pt loading compared to blanket deposition while still maintaining electrical continuity, leading to possible improvements in fuel cell performance.

In these studies, micropatterned Pt grid structures were integrated into the SOFCs as current collectors. For this purpose, an array of 16 lanthanum−strontium−iron−cobalt oxide, $La_{0.6}Sr_{0.4}Co_{0.2}Fe_{0.8}O_{3-\delta}$ (LSCF), cathodes was deposited onto 50 μm thick commercial YSZ plates by pulsed laser deposition (PLD) with a physical shadow mask. The LSCF film deposited in this way is quite dense.[23] Pt current collector grids were then applied onto the LSCF cathodes by area-selective atomic layer deposition, aligned with the aid of a microscope. On the other side of the YSZ plate, a 80 nm thick dc-sputtered Pt layer served as the anode.

In order to generate the Pt grid pattern for the SOFC current collector, we used the microcontact printing (μCP) method to achieve area-selective ALD.[16–18] In this method, an octadecyltrichlorosilane (ODTS) monolayer is transferred to the substrate in the desired pattern using a prefabricated PDMS stamp. For this process, the Pt ALD conditions were modified slightly. Compared to the regular Pt ALD process, we used an expanded purging time of 30 s to ensure removal of any unreacted precursor from the substrate while using the same precursor dose times and temperature settings. The optimization procedures for the area-selective ALD experiments have been reported previously.[16–18]

To cast the PDMS stamps, a Si master was fabricated though conventional photolithography with a layer of photoresist of thickness 7 μm. The PDMS stamp was peeled off from the Si master once the PDMS stamp was cured. To achieve an excellent area-selective ALD process, high-quality patterned ODTS films have to be deposited, via the PDMS stamp, to block the oxygen-containing active sites present on the substrate.[16–18,29,30] Thus, the quality of the PDMS stamp is regarded as a key element of the microcontact printing procedure since it directly determines the quality of the ODTS pattern and consequently the quality of the micropatterned Pt structures. Both SEM and AFM were used to examine the quality of the PDMS stamp (desired pattern consist of 4 μm × 2 μm grids). Figure 7a is an SEM image of the PDMS stamp showing evenly distributed 5 μm × 5 μm squares which are clearly separated by 1 μm wide lines; the deviation from the desired 4 μm × 2 μm dimension is due to overexposure in the fabrication of the Si master. The SEM image reveals that the corner of each square is rounded to some degree; we believe this is also due to overexposure during the Si master fabrication process. AFM section analysis in Figure 7b indicates that a regular pattern has been achieved. Although the stamp is not perfect, it still works well for our procedure to fabricate the micropatterned Pt structure because the ODTS-free areas for Pt ALD growth are connected and it will produce electrically connected Pt current grids as a result of the area-selective ALD process.

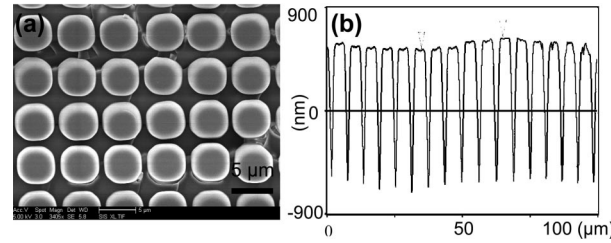

Figure 7. (a) SEM image of the PDMS stamp used in the area-selective ALD experiments. (b) AFM cross-sectional analysis of the PDMS stamp.

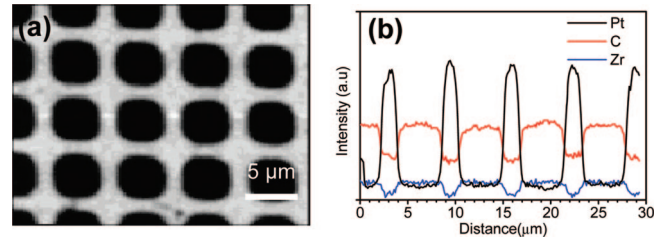

Figure 8. (a) Auger electron spectroscopy elemental maps for platinum on the micropatterned grid structure after area-selective ALD of Pt on YSZ. (b) Defined AES line scan showing alternation of Pt, C, and Zr signals.

Using microcontact printing, the pattern encoded in the PDMS stamp is transferred via application of the ODTS SAM onto the substrate, and Pt thin films are selectively deposited by ALD onto the areas of the substrate that are not deactivated by ODTS. Auger electron spectroscopy (AES) was used to probe the micropatterned Pt structures on the YSZ substrates formed by this process. Figure 8a shows the AES elemental mapping of Pt carried out on the micropatterned Pt structure. In the AES map, the relative elemental peak intensity is presented as the pixel brightness. The brighter the spot, the larger the amount of the element present on the surface. In Figure 8a, the bright regions indicate the presence of Pt while the dark areas indicate the absence of Pt. Pt clearly is deposited only in the desired grid pattern. Figure 8b shows an Auger line scan of the peak intensities of Pt, C, and Zr along a defined line across the patterned Pt structure. The Auger peaks of Pt, C, and Zr exhibit the expected intensity alternation, and no Pt deposition[31] is detected at the ODTS-coated areas. The carbon line scan in Figure 8b (red line) indicates that carbon is observed on the Pt-coated regions of the patterned substrate, which is believed to come from adventitious carbon arising from the ex situ analysis. Both the Auger line scan and the Auger elemental mapping confirm that the Pt patterns were well defined and directed with high selectivity by the patterned SAMs generated with microcontact printing. The micropatterned Pt grid structure constitutes a current collector for the fuel cell.

(29) Chen, R.; Kim, H.; McIntyre, P. C.; Bent, S. F. *Appl. Phys. Lett.* **2004**, *84*, 4017.
(30) Chen, R.; Kim, H.; McIntyre, P. C.; Bent, S. F. *Chem. Mater.* **2005**, *17*, 536.

(31) The absolute signal at the Pt Auger electron energy selected for the line scan did not go to zero due to contributions from an overlapping Zr satellite peak; however, examination of the entire survey scan confirms that Pt is not present.

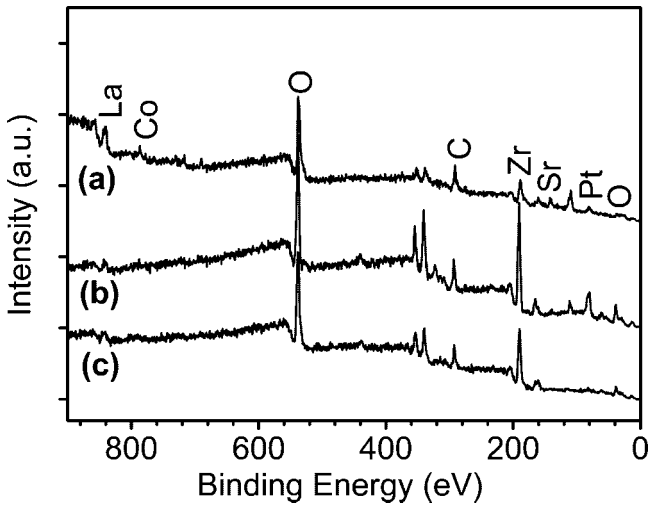

Figure 9. XPS spectra after Pt ALD onto (a) cathode material LSCF patterned with the ODTS grid, (b) bare YSZ substrate, (c) continuous ODTS-coated YSZ. The ALD conditions used here: substrate temperature, 285 °C; Pt precursor temperature, 65 °C; Pt precursor and air pulse time, 2 s; nitrogen purging time, 30 s; ALD cycles, 50. Note: C comes from environment contamination.

Before we integrated the micropatterned Pt structures onto the SOFCs, we also probed the selectivity of Pt ALD directly on the cathode material LSCF using XPS. Figure 8 shows the XPS spectra of the ALD Pt on three different samples: (a) a patterned ODTS-coated LSCF substrate, (b) a bare YSZ substrate, and (c) a continuous ODTS-coated YSZ substrate. Although involving two different substrates (YSZ and LSCF), a comparison of the amount of Pt deposition in the three areas allows us to check qualitatively whether the area-selective ALD process is successful on the LSCF sample. The Pt atomic percentages measured for these three samples are 0.9%, 2.6%, and <0.1%, respectively (here 0.1% is the sensitivity limit for XPS). Two ratios will be compared to characterize the blocking effectiveness of ODTS against Pt ALD onto the cathode material LSCF. The ratio of at. % Pt on the ODTS patterned LSCF sample (Figure 9a) to at. % Pt on the nondeactivated YSZ sample (Figure 9b) is 34.6%, while within the patterned sample measured for Figure 9a, the percentage of the bare LSCF area in each repeating unit is 36%. This is the fractional area that would be expected to be Pt coated if perfect selectivity were achieved. These two values are close to each other, illustrating that the selectivity of Pt onto the cathode material LSCF is very good.

After depositing the Pt grid pattern on LSCF, the SOFC performance was characterized. Figure 10 shows the $I-V$ and $I-P$ curves of the fuel cells with and without Pt current collector grids, at a thickness of 4.5 nm, on the cathode side. As mentioned earlier, the 4.5 nm ALD-deposited Pt film has a resistivity of 51 $\mu\Omega\cdot$cm, somewhat higher than the thicker Pt films; this higher resistivity is not expected to be a problem during these cathode experiments, however, since (1) it is deposited on top of LSCF, which is conductive, and (2) there is no production of water at the interface of the cathode and electrolyte during the fuel cell operation which might degrade the

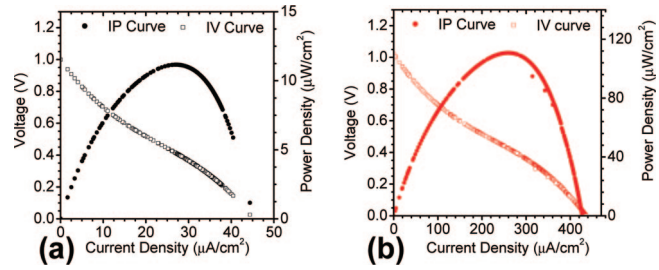

Figure 10. $I-V$ and $I-P$ characteristics of fuel cells (a) without and (b) with Pt current collector grids. Starting fuel cell structure: PLD LSCF 20 nm (cathode)/commercial YSZ plate 50 μm (electrolyte)/dc-sputtered Pt 80 nm (anode). Both measurements are done at 350 °C with a fuel flow rate of 10 sccm. ALD conditions used here: substrate temperature, 285 °C; Pt precursor, 65 °C; Pt precursor and air pulse time, 2 s; nitrogen purging time, 30 s; ALD cycles, 100.

film. The starting fuel cell structure is pulsed laser deposited LSCF of 20 nm thickness (cathode)/commercial YSZ plate of 50 μm thickness (electrolyte)/dc-sputtered Pt of 80 nm thickness (anode). Compared to the peak power densities measured for the fuel cells used in the experiments of optimal anode film thickness (measured as high as 45 mW/cm^2), the power densities here are much lower (in the μW/cm^2 range). This difference is due to the significantly thicker electrolyte (50 μm vs 100 nm), resulting in huge ohmic losses which reduce the fuel cell performance significantly. From Figure 10a and 10b, we observe that the open-circuit voltages of the two fuel cells are almost the same value of 1.0 V, but the peak power densities of the two fuel cells are 11.2 and 110.7 μW/cm^2 for the fuel cell without and with current grids, respectively. It is apparent that by employing the Pt current collector grids, the fuel cell performance is improved by a factor of 10. Because the pulse laser-deposited LSCF film is dense,[23] we can exclude the possibility that diffusion and deposition of Pt on the LSCF pores toward the electrode/electrolyte interface improve SOFC performance. Consequently, we suggest that the positive impact achieved after applying ALD Pt current collecting grids results from the following two possible contributions. One is that addition of the Pt component facilitates the oxygen dissociative adsorption onto the cathode material LSCF, thus speeding up the electrode reaction, i.e., a catalytic effect. The other is that it increases the fuel cell performance by collecting more current from the cathode. Given the catalytic nature of Pt, it would be interesting to deposit another noncatalytic metal, such as Au, as the current collector to separate the influence of catalytic and electronic effects on LSCF cathode improvement.

Conclusions

In this work, we demonstrated a way to fabricate Pt thin films of high purity and low resistivity onto SOFC's using the ALD technique. In addition, patterned Pt thin films with high spatial resolution, as small as 2 μm, have been achieved on YSZ substrates using a combined μCP and ALD method. Furthermore, we successfully integrated both Pt thin films and Pt grid structures into working fuel cells. From the characterization of the fuel cell perfor-

mance, we show that ALD-deposited Pt thin films can work as a good electrode material and also that the Pt current collector grids enable significant improvement in the fuel cell performance. However, some loss of fuel cell performance was observed, which is attributed in part to the degradation of the fuel cell catalyst. We are actively researching better catalysts to enhance the thermal and microstructural stability.

The ALD-deposited Pt thin films and micropatterned Pt structure introduced here can potentially be integrated onto any type of fuel cell as a catalyst layer to improve the electrode reaction and as a current collector to improve the current collection efficiency. To make full use of the advantages of ALD-deposited Pt films, such as high conformality and low resistivity for films as thin as 5 nm, better catalyst−support geometries should be designed for coating Pt through atomic layer deposition

Acknowledgment. The authors are grateful to Joon Hyun Shim and Cheng-Chieh Chao for providing YSZ substrates and fuel cell test structures and to Kevin Crabb for depositing LSCF for the fuel cell samples.

CM7033189